

## IRON-RICH EJECTA IN THE SUPERNOVA REMNANT DEM L71

JOHN P. HUGHES<sup>1</sup>, PARVIZ GHAVAMIAN<sup>1</sup>, CARA E. RAKOWSKI<sup>1</sup>, AND PATRICK O. SLANE<sup>2</sup>,  
*Received 2002 November 20; accepted 2002 December 4*

### ABSTRACT

*Chandra* X-ray observations of DEM L71, a supernova remnant (SNR) in the Large Magellanic Cloud (LMC), reveal a clear double shock morphology consisting of an outer blast wave shock surrounding a central bright region of reverse-shock heated ejecta. The abundances of the outer shock are consistent with LMC values, while the ejecta region shows enhanced abundances of Si, Fe, and other species. However, oxygen is not enhanced in the ejecta; the Fe/O abundance ratio there is  $\gtrsim 5$  times the solar ratio. Based on the relative positions of the blast wave shock and the contact discontinuity in the context of SNR evolutionary models, we determine a total ejecta mass of  $\sim 1.5 M_{\odot}$ . Ejecta mass estimates based on emission measures derived from spectral fits are subject to considerable uncertainty due to lack of knowledge of the true contribution of hydrogen continuum emission. Maximal mass estimates, i.e., assuming no hydrogen, result in  $1.5 M_{\odot}$  of Fe and  $0.24 M_{\odot}$  of Si. Under the assumption that an equal quantity of hydrogen has been mixed into the ejecta, we estimate  $0.8 M_{\odot}$  of Fe and  $0.12 M_{\odot}$  of Si. These characteristics support the view that in DEM L71 we see Fe-rich ejecta from a Type Ia SN several thousand years after explosion.

*Subject headings:* ISM: individual (DEM L71, 0505–67.9) – nuclear reactions, nucleosynthesis, abundances – shock waves – supernova remnants – X-rays: ISM

### 1. INTRODUCTION

A distinguishing characteristic of Type Ia supernovae (SNe) is the large amount of iron that they are thought to produce mainly through the decay of radioactive Ni<sup>56</sup>. The nuclear decay of this material powers the SN light curve, thereby providing a constraint on the quantity of material ejected in individual SN events. Although variation in the amount and distribution of radioactive ejecta likely accounts for the modest range of peak absolute magnitudes seen in Type Ia SNe, by and large SNe Ia are strikingly homogeneous in their properties. Various observational constraints (e.g., the absence of hydrogen in optical spectra near optical maximum, occurrence in older stellar populations, and the relatively large amount of Ni<sup>56</sup> produced) have led to the current framework involving carbon deflagration/detonation in a white dwarf driven to the Chandrasekhar limit by accretion. The most likely progenitor system (Branch et al. 1995) is a C-O white dwarf accreting H/He-rich gas from a companion, either from its wind or through Roche lobe overflow. Remnants of SN Ia should contain about one Chandrasekhar mass of ejecta comprised of 0.6–0.8  $M_{\odot}$  of iron with intermediate-mass elements (O, Mg, Si, S, Ca) distributed in the outer layers (e.g., Iwamoto et al. 1999). Current models predict that SNe Ia should leave no compact remnant.

One of the goals of supernova remnant (SNR) research has been to use remnant properties to infer the nature of the progenitor. Such properties as the partially neutral nature of the surrounding ambient medium (Tuohy et al. 1982) or the Fe-rich composition of the ejecta (Hughes et al. 1995) have been used to argue for a SN Ia origin for some SNRs. In this article we investigate the Large Magellanic Cloud (LMC) SNR DEM L71 (0505–67.9) which exhibits both of these features. DEM L71 (Davies, El-

liott, & Meaburn 1976) was first proposed as a supernova remnant based on the *Einstein* X-ray survey of the LMC (Long, Helfand, & Grabelsky 1981). Follow-up optical spectroscopy confirmed this identification and revealed the remnant to be Balmer-dominated (Tuohy et al. 1982; Smith et al. 1991), that is to say, one whose optical spectrum is dominated by hydrogen emission with little or no emission from forbidden lines of [O III] or [S II]. The remnants of Tycho's SN and SN1006 are Galactic examples of such SNRs (Kirshner & Chevalier 1978; Schweizer & Lasker 1978). *ASCA* X-ray studies of DEM L71 (Hughes, Hayashi, & Koyama 1998) yielded an age of  $\sim 5000$  yr and evidence for the presence of SN ejecta in the form of an enhanced global abundance of Fe. Here we present results from new *Chandra* observations of the remnant that bear closely on the nature of the originating SN.

### 2. ANALYSIS

We observed DEM L71 using the back-side-illuminated chip (S3) of the Advanced CCD Imaging Spectrometer (ACIS-S) instrument in full-frame timed exposure mode starting on 2000 January 04 for 45.4 ks (OBSID 775). The reduction of these data proceeded as described in Rakowski et al. (2002). Our H $\alpha$  image was constructed from a subset of a 3-D position-velocity data cube obtained on DEM L71 using the Rutgers Fabry-Perot (RFP) at the focus of the CTIO 1.5-m on 1998 February 18. The RFP data reduction is described in Ghavamian et al. (2002).

#### 2.1. Spatial

The soft X-ray image of DEM L71 from *Chandra* (Fig. 1, middle panel) shows emission from an egg-shaped outer rim that matches nearly perfectly the optical H $\alpha$  image (Fig. 1, left panel). Features in common include matched variations in surface brightness around the rim as well as

<sup>1</sup> Department of Physics and Astronomy, Rutgers University, 136 Frelinghuysen Road, Piscataway, NJ 08854-8019

<sup>2</sup> Harvard-Smithsonian Center for Astrophysics, 60 Garden Street, Cambridge, MA 02138

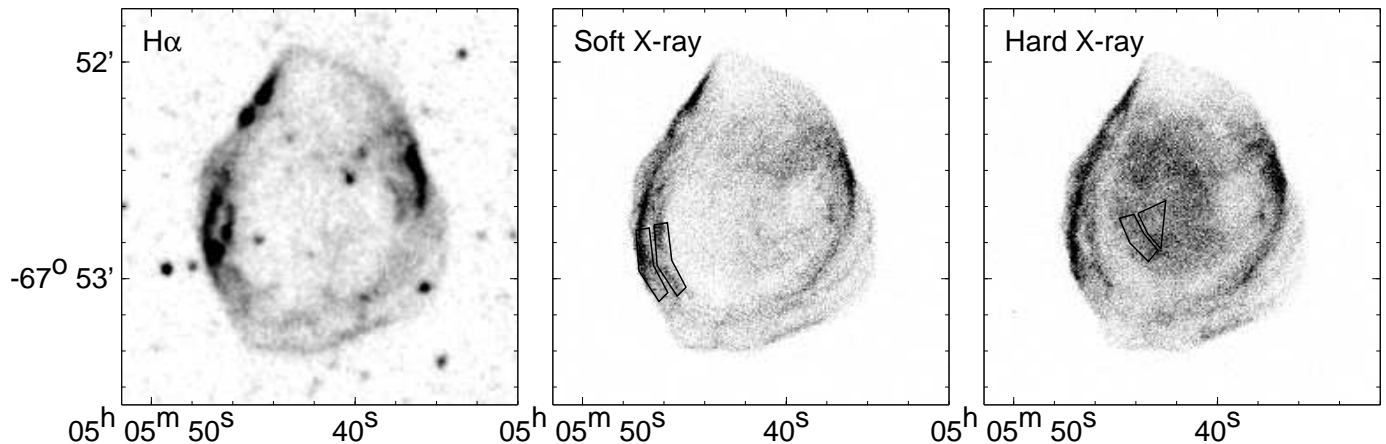


FIG. 1.— Images of the supernova remnant DEM L71 in  $H\alpha$  (left panel); *Chandra* soft X-ray (0.2–0.7 keV) (middle panel); and *Chandra* hard X-ray band (0.7–2.6 keV) (right panel). North is up and east is to the left; axes are labelled in epoch J2000. The grayscale intensity scaling is linear in all panels. Spectral extraction regions are superposed on the soft and hard X-ray images.

the presence of multiple nested filaments, which are particularly noticeable along the southern edge. Faint diffuse emission in the interior of the SNR agrees well too. The remarkable detailed similarity of the X-ray and optical morphology is uncommon among supernova remnants in general. Nearly all of the optical emission in DEM L71 arises in high velocity (500–1000 km s<sup>-1</sup>) nonradiative shocks, with little contribution from the slow ( $\sim 100$  km s<sup>-1</sup>) radiative shocks typically seen in middle-aged remnants. Furthermore the X-ray emission shows broadly similar intrinsic emissivities around the rim (there are no large variations in abundance or thermodynamic state, see Rakowski, Ghavamian, & Hughes 2002) so that surface brightness variations largely trace variations in the ambient gas density around the remnant. North-south the outer rim spans 83'', while in the east-west direction it is only 60'' across. Any differences between the X-ray and optical sizes are small, no more than a 0.5'' difference in diameter, with the optical dimensions being marginally larger than the X-ray ones.

The hard X-ray image of DEM L71 (Fig. 1, right panel) shows emission from the outer rim that resembles the soft X-ray and  $H\alpha$  images. However, this band also reveals a new spatial component of X-ray emission that has no counterpart in the other bands. This emission almost fills the interior and appears as a modestly limb-brightened, elliptical shell of emission slightly offset from the geometric center of the outer rim. The emission extends 40'' by 32'' at a position angle (for the major axis) of  $\sim 12^\circ$  east of north and is centered at  $05^{\text{h}}05^{\text{m}}42.6^{\text{s}} - 67^\circ 52'38.6''$  (J2000). Hereafter we refer to this as the “core” emission.

## 2.2. Spectral

Spectra were extracted from four regions in the remnant’s southeastern quadrant (see figure 1) to investigate the soft and hard X-ray emission components. Two spectra of the soft rim (“outer” and “inner”), corresponding to the two nested filaments that appear here, were extracted. Likewise two spectra of the core X-ray emission (again “outer” and “inner”) were extracted. Background-subtracted count rates are given in Table 1. Background represented less than 0.5% of the source count rate in the

0.2–5 keV band as taken from a 1'–2' annulus outside the remnant. Before fitting, source spectra were rebinned to a minimum of 10 counts per channel. The rim data sets (2 left panels of fig. 2) are quite similar as are the core data sets (2 right panels), but the rim and core spectra differ significantly from each other.

The abundances and emission properties of the gas were constrained through fits of nonequilibrium ionization (NEI) planar-shock thermal plasma models (see Hughes, Rakowski, & Decourchelle 2000). The abundances of O, Ne, Mg, Si, S, and Fe were allowed to vary, while C, N, Ar and Ca were fixed at 20% of solar and the Ni abundance was tied to Fe. The fits were generally acceptable with similar best-fit values for similar regions (see Table 1). Absorption of low energy X-rays by intervening gas and dust was included with the hydrogen column density,  $N_{\text{H}}$ , as a free parameter. The values obtained,  $N_{\text{H}} = 4\text{--}7 \times 10^{20}$  atoms cm<sup>-2</sup>, are consistent with previous X-ray spectral fits (Hughes et al. 1998) and the Galactic H I column density in this direction (Dickey & Lockman 1999).

TABLE 1  
NEI THERMAL MODEL FITS FOR REGIONS IN DEM L71

Parameter	Outer rim	Inner rim	Outer core	Inner core
Rate (s <sup>-1</sup> )	0.29	0.20	0.098	0.093
$N_{\text{H}}$ ( $10^{21}$ cm <sup>-2</sup> )	$0.58^{+0.04}_{-0.06}$	$0.41^{+0.04}_{-0.04}$	$0.67^{+0.31}_{-0.17}$	$0.52^{+0.24}_{-0.14}$
$kT$ (keV)	$0.47^{+0.03}_{-0.03}$	$0.47^{+0.03}_{-0.04}$	$1.6^{+0.7}_{-0.5}$	$1.1^{+0.3}_{-0.3}$
$\log(n_e t / \text{cm}^{-3}\text{s})$	$11.64^{+0.11}_{-0.11}$	$11.66^{+0.15}_{-0.20}$	$10.80^{+0.22}_{-0.16}$	$11.00^{+0.31}_{-0.16}$
O	$0.21^{+0.03}_{-0.02}$	$0.13^{+0.02}_{-0.01}$	$0.31^{+0.25}_{-0.09}$	$0.33^{+0.27}_{-0.09}$
Ne	$0.42^{+0.05}_{-0.04}$	$0.34^{+0.04}_{-0.03}$	$2.3^{+1.9}_{-0.9}$	$1.7^{+1.5}_{-0.8}$
Mg	$0.37^{+0.08}_{-0.07}$	$0.24^{+0.07}_{-0.07}$	$1.7^{+1.6}_{-0.7}$	$1.1^{+1.2}_{-0.5}$
Si	$0.33^{+0.11}_{-0.11}$	$0.23^{+0.14}_{-0.12}$	$0.7^{+1.0}_{-0.5}$	$1.0^{+1.1}_{-0.5}$
S	$0.06^{+0.30}_{-0.06}$	< 0.30	< 2.6	< 2.1
Fe	$0.093^{+0.012}_{-0.009}$	$0.079^{+0.010}_{-0.009}$	$1.9^{+1.4}_{-0.6}$	$1.7^{+1.2}_{-0.6}$
$\chi^2/\text{d.o.f}$	103.1/100	79.4/91	85.6/73	102.6/69

The ionization timescale of the rim region indicates that the gas is out of equilibrium, as expected. The fitted abundances are sub-solar and generally consistent with the gas phase LMC values (Russell & Dopita 1992). The Fe abundance is derived from the L-shell lines that produce, at CCD spectral resolution, a quasi-continuum blend of emission over the 0.7–1.5 keV band. Note that our NEI spectral model is derived from the original Raymond & Smith

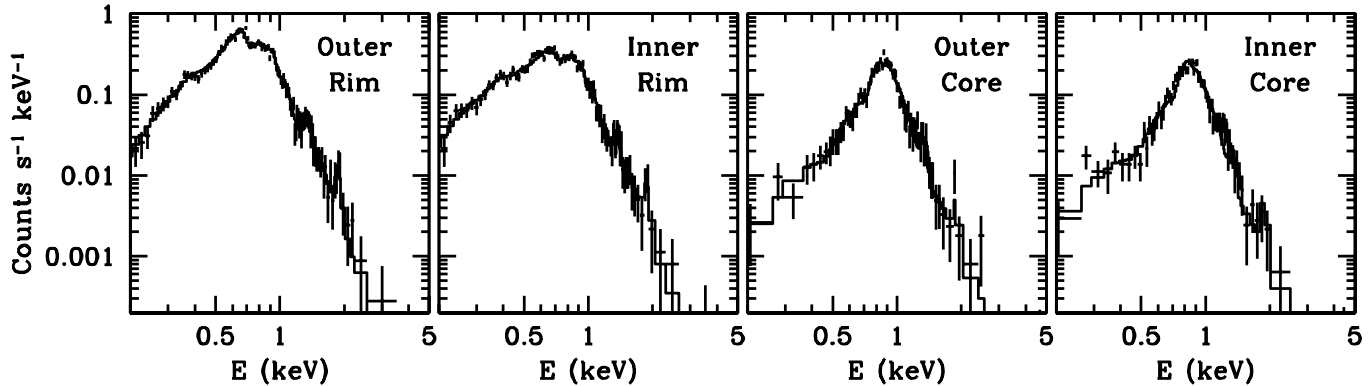


FIG. 2.— X-ray spectra extracted from several locations in the southeastern quadrant of DEM L71 with best-fit nonequilibrium ionization thermal plasma emission models.

(1977) code (and subsequent revisions) which accurately models the overall flux of the Fe L-shell emission, but is less accurate at modeling its detailed spectral variation with photon energy, due to limitations in the availability of atomic data. This is the case to a greater or lesser extent for all NEI spectral models currently available. Typically with such models, the fitted Fe abundance is low, while the abundances of Ne and Mg, whose K-shell lines fall in this energy band, are enhanced to compensate for deficiencies in the modeled Fe L-shell emission. Nevertheless these spectral fits (as well as the more comprehensive study of DEM L71’s outer rim in Rakowski et al. 2002) confidently confirm that the rim region is swept-up interstellar medium (ISM) heated to X-ray emitting temperatures by a high velocity blast wave. We note that there is no evidence for a hard power-law tail beyond the thermal emission in the *Chandra* spectrum of the rim.

In marked contrast to the rim regions, the core spectra are dominated by the Fe L-shell blend, which peaks near 0.8 keV, and have no significant O line emission at  $\sim 0.65$  keV. The fitted parameters (Table 1) reveal that the abundances of all species, with the exception of O, are considerably greater than the LMC mean, while the abundances of some species, Ne and Fe in particular, are even greater than solar. The abundance ratio of iron to oxygen is  $\gtrsim 5$  times the solar ratio. These large absolute abundances, in addition to the non-solar abundance ratios, signal the presence of supernova ejecta in the core of the remnant.

### 3. EJECTA MASS

Here we quantitatively examine the properties of the core region to identify the evolutionary state of the remnant and the nature of the originating SN. The large iron-to-oxygen ratio of the core X-ray emission, as well as its highly-symmetric, well-ordered spatial distribution, immediately suggests a SN Ia origin for DEM L71. A critical diagnostic of the SN type is the total mass of ejecta. We estimate this in two ways, first using dynamical considerations and then from the properties of the core X-ray emission.

The position of the reverse shock (or contact discontinuity) relative to that of the blast wave can constrain the evolutionary state of a remnant in the context of self-

similar models (e.g., Truelove & McKee 1999). Once the profiles of the ISM and ejecta are chosen, this constraint is unique. Although subject to hydrodynamic instabilities, the position of the contact discontinuity between the SN ejecta and the ambient medium is reasonably well identified in our image — it is marked by the outer extent of the core hard emission. This has a geometric mean radius of 4.3 pc assuming an LMC distance of 50 kpc. DEM L71’s outer blast wave has a geometric mean radius of 8.6 pc, yielding a ratio for the radii of  $\sim 2$ .

In their study of instabilities and clumping in SNe Ia, Wang & Chevalier (2001) present the 1-D radial evolution of the contact discontinuity and blast wave for an exponential ejecta density profile interacting with a constant density ambient medium. For this model, the radius of the contact discontinuity is approximately one-half that of the blast wave when the normalized radius of the forward shock is  $r' \sim 3$ . The physical radius of the forward shock,  $r$ , depends on the normalized radius,  $r'$ ; the ejected mass,  $M$ ; and the ambient hydrogen number density,  $n_0$ , through a scaling relation. Inverting, we obtain a relation for the ejected mass in terms of the Chandrasekhar mass,  $M_{\text{ch}}$

$$M = M_{\text{ch}} n_0 \left( \frac{r/1 \text{ pc}}{2.19 r'} \right)^3.$$

which evaluates to  $M \sim 1.1 M_{\text{ch}}$  for  $r' = 3$ ,  $r = 8.6$  pc and a mean ambient density of  $0.5 \text{ cm}^{-3}$  (Ghavamian et al. 2002). At this time the entire ejecta have been thermalized, the reverse shock has just reached the center, and the ejecta are moving outward relatively slowly at  $\lesssim 100 \text{ km s}^{-1}$ .

For our second ejecta mass estimate, we extracted spatially resolved spectra of the core from five concentric elliptical rings spaced by  $5''$  (in semi-major axis length). The annuli had constant ellipticity (an axial ratio of 1.25) and position angle ( $12^\circ$  east of north). Each of these spectra contain projected emission from the blast wave, which we removed by subtracting off a spectrum of the bright rim emission scaled independently for each annular ring to zero out the resultant spectrum over the 0.2–0.6 keV band. This band was chosen because it shows no evidence for enhanced central emission and thus plausibly corresponds to emission from the blast wave alone. The count

rates of the various spectra range from  $0.068 \text{ s}^{-1}$  to  $0.38 \text{ s}^{-1}$ .

These spectra all show the broad Fe L-shell blend and clearly resolved Si and S  $K\alpha$  lines, but no obvious  $K\alpha$  lines of O, Ne, or Mg. We fit these spectra with the NEI spectral model including a minimal set of elemental species: Si, S, Ar, Ca, Fe, Ni, and a H continuum. To further simplify the model we restricted the number of free parameters in the fits. The global NEI parameters, temperature and ionization timescale, and the Ni to Fe ratio were constrained to be the same for all five spectra. We allowed the emission measures (EMs) of Si and Fe to vary freely in all the spectra; however, the S, Ar, and Ca EMs varied along with Si at their relative solar abundance ratios. EMs are defined as  $n_e n_i V$ , where  $n_e$  and  $n_i$  are the electron and ion number densities and  $V$  is the emitting volume. We fit both the low ( $E < 1.5 \text{ keV}$ ) and high ( $E > 1.5 \text{ keV}$ ) energy portions of the spectra separately in order to ensure that the fits were not being dominated by the “shape” of the Fe L-shell blend. In fact both portions of the spectra are broadly consistent with  $kT \sim 1 \text{ keV}$  and  $\log(n_e t / \text{cm}^{-3}) \sim 11.2$ . Finally the fits were performed for three values of the column density,  $N_H = (4, 8, 12) \times 10^{20} \text{ atoms cm}^{-2}$ , fixed separately for three different sets of fits, in order to estimate uncertainties on the parameters. The fits are not particularly good from a  $\chi^2$  point-of-view, but most of the residuals are associated with the Fe-L shell blend.

From the fits we obtain numerical values for the EMs of the Fe and Si-group elements as a function of radius in the core region. For simplicity we assume spherical geometry for the deprojection. If the true 3-D shape of the core region were ellipsoidal, then our mass estimates would be some 13% higher (prolate) or lower (oblate). We assume that the Fe and Si-group components are co-spatial, although we allow for the components to contribute in differing proportions in each radial shell. The mean charge state of each species in the fit is calculated using the values quoted above for  $kT$  and  $n_e t$ . For example, the mean number of electrons per ion is 11.8 for Si and 18.2 for Fe.

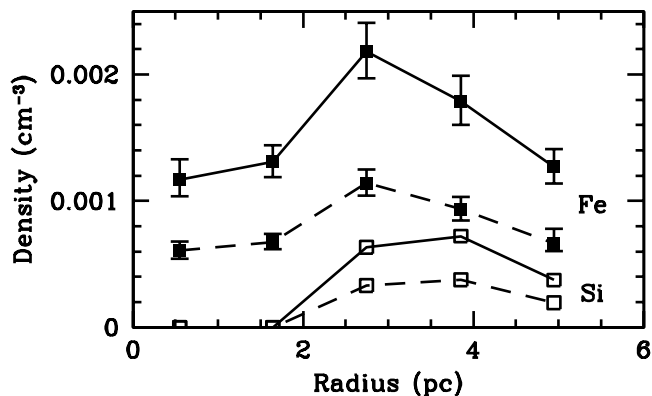


FIG. 3.— Deprojected Fe and Si number densities as a function of radius in the ejecta of DEM L71. The curves with solid (open) symbols correspond to the Fe (Si) density. Solid curves are the maximal density estimates; dashed curves assume an equal mass of hydrogen mixed into the ejecta (see text). Error bars show the effect of varying the hydrogen column density (not plotted for Si, since these errors are smaller than the size of the points).

The main uncertainty in converting EMs to Fe and Si density and mass estimates is not knowing which species

contribute electrons. In a solar abundance plasma, there are  $\sim 3 \times 10^4$  electrons (mostly from hydrogen) per Fe ion, compared to the roughly 50 electrons per Fe ion in a pure metal plasma. Thus if even just a small quantity of hydrogen were mixed into the ejecta, it would drastically affect the derived densities. Our spectral fits are inconclusive regarding the amount of hydrogen present in the core region. The spectral fits discussed here require a relatively high level of broadband continuum emission, yet in other fits we performed a wide range of continuum intensities were inferred, while the EMs of the metals remained fairly stable. Furthermore, although we have modeled a hydrogen continuum, any fully stripped ion could produce the requisite featureless spectrum. Thus in lieu of a definitive result we present a couple of astrophysically plausible estimates. For one we assume that the metals are the sole source of electrons, which yields maximal density estimates. For the other we make the plausible assumption that a comparable mass of hydrogen has been well mixed into the metal rich ejecta during its evolution.

The deprojected Fe and Si densities versus radius are plotted in figure 3. Each clearly shows enhanced density around 3–4 pc indicating a thick shell structure with the Si slightly ahead of the Fe. Fe is present even in the center of the remnant, while Si is absent there. Integrating the density profiles we obtain total masses of  $1.5 M_\odot$  of Fe and  $0.24 M_\odot$  of Si assuming a pure metal composition for the emitting material. The curves for the case with a modest admixture of hydrogen are quite similar in shape to those of the pure metal case (see figure 3), although the ion densities we infer are about a factor of two lower. The total amount of Fe is  $0.8 M_\odot$  and that of Si is  $0.12 M_\odot$ .

#### 4. SUMMARY

The spatial and spectral analysis of the *Chandra* ACIS data reveal DEM L71 to be a textbook example of a supernova remnant: an outer blast wave shock propagating through the ISM that surrounds a core of SN ejecta heated to X-ray-emitting temperatures by the inward moving reverse shock. Our analysis strongly argues for a Type Ia SN origin for DEM L71. Specifically we find (1) a large Fe to O ratio in the ejecta X-ray emission; (2)  $\sim 1.5 M_\odot$  of ejecta from dynamical considerations; (3) a relatively low mass ratio of Si to Fe ( $\sim 0.15$ ); and (4) a large mass of ejected Fe ( $\sim 0.8 M_\odot$ ). These results are all consistent with SN Ia ejecta and further may have some power to discriminate between models for how the flame front propagates in these explosions (see, e.g., Iwamoto et al. 1999). The ejecta are mostly contained within a thick shell and are partially stratified. According to our deprojection analysis, Fe extends throughout the entire ejecta even into the center, while Si appears to be contained only within the outer half of the ejecta.

A considerably deeper *Chandra* observation of DEM L71 has been approved for observation in cycle 4. This will allow us to search for and study spectral variations within the Fe-rich ejecta and to determine its morphology in greater detail. Measuring the kinematics of the Fe-rich ejecta is an important next step. Unfortunately this is likely to be beyond the capabilities of *Chandra*, *XMM-Newton*, and even *Astro-E2*, although the Constellation-X Facility, if it attains angular resolution of  $10''$ , should be

able to detect the expected motions of  $\sim 100 \text{ km s}^{-1}$ . We are also pursuing ground-based optical searches for coronal [Fe XIV]  $\lambda 5303 \text{ \AA}$  line emission from the ejecta, which could provide complementary insights into the nature and dynamics of the ejecta.

We thank Ted Williams for assistance with the Fabry-

Perot observations, Leisa Townsley for allowing us to use her CTI corrector software, and John Nousek and Dave Burrows for help with the original proposal. Partial financial support was provided by NASA contract NAS8-39073 (SAO), *Chandra* grants GO0-1035X and GO1-2052X (Rutgers), and a NASA Graduate Student Researchers Program fellowship to CER.

#### REFERENCES

- Davies, R. D., Elliott, K. H., & Meaburn, J. 1976, *MmRAS*, 81, 89  
 Dickey, J. M., & Lockman, F. J., 1990, *ARAA*, 28, 215  
 Dwarkadas, V. V., & Chevalier, R. A. 1998, *ApJ*, 497, 807  
 Ghavamian, P., Rakowski, C. E., Hughes, J. P., & Williams, T. B. 2002, *ApJ*, submitted.  
 Hughes, J. P., Hayashi, I., & Koyama, K. 1998, *ApJ*, 505, 732  
 Hughes, J. P., Rakowski, C. E., & Decourchelle, A. 2000, *ApJ*, 543, L61  
 Iwamoto, K., Brachwitz, F., Nomoto, K., Kishimoto, N., Umeda, H., Hix, W. R., & Thielemann, F. 1999, *ApJS*, 125, 439  
 Kirshner, R. P., & Chevalier, R. A. 1978, *A&A*, 67, 267  
 Long, K. S., Helfand, D. J., & Grabelsky, D. A. 1981, *ApJ*, 248, 925  
 Rakowski, C. E., Ghavamian, P., & Hughes, J. P. 2002, *ApJ*, submitted.  
 Raymond J. C., & Smith, B. W. 1977, *ApJS*, 35, 419  
 Russell, S. C., & Dopita, M. A. 1992, *ApJ*, 384, 508  
 Schweizer, F., & Lasker, B. M. 1978, *ApJ*, 226, 167  
 Smith, R. C., Kirshner, R. P., Blair, W. P., & Winkler, P. F. 1991, 375, 652.  
 Truelove, J. K., & McKee, C. F. 1999, *ApJS*, 120, 299 (erratum: *ApJS*, 128, 403)  
 Wang, C.-Y., & Chevalier, R. A. 2001, *ApJ*, 549, 1119